Biophysical Journal

Article



Fibrillation of Human Calcitonin and Its Analogs: Effects of Phosphorylation and Disulfide Reduction

Harshil K. Renawala, Karthik B. Chandrababu, and Elizabeth M. Topp^{1,2,*}

¹Department of Industrial and Physical Pharmacy, College of Pharmacy, Purdue University, West Lafayette, Indiana and ²National Institute for Bioprocessing Research and Training, Dublin, Ireland

ABSTRACT Some therapeutic peptides self-assemble in solution to form ordered, insoluble, β -sheet-rich amyloid fibrils. This physical instability can result in reduced potency, cause immunogenic side effects, and limit options for formulation. Understanding the mechanisms of fibrillation is key to developing rational mitigation strategies. Here, amide hydrogen-deuterium exchange with mass spectrometric analysis (HDX-MS) coupled with proteolytic digestion was used to identify the early stage interactions leading to fibrillation of human calcitonin (hCT), a peptide hormone important in calcium metabolism. hCT fibrillation kinetics was sigmoidal, with lag, growth, and plateau phases as shown by thioflavin T and turbidity measurements. HDX-MS of fibrillating hCT (pH 7.4; 25°C) suggested early involvement of the N-terminal (1–11) and central (12–19) fragments in interactions during the lag phase, whereas C-terminal fragments (20–32 and 26–32) showed limited involvement during this period. The residue-level information was used to develop phosphorylated hCT analogs that showed modified fibrillation that depended on phosphorylation site. Phosphorylation in the central region resulted in complete inhibition of fibrillation for the phospho-Thr-13 hCT analog, whereas phosphorylation in the N-terminal and C-terminal regions inhibited but did not prevent fibrillation. Reduction of the Cys1-Cys7 disulfide bond resulted in faster fibrillation with involvement of different hCT residues as indicated by pulsed HDX-MS. Together, the results demonstrate that small structural changes have significant effects on hCT fibrillation and that understanding these effects can inform the rational development of fibrillation-resistant hCT analogs.

SIGNIFICANCE Amide hydrogen-deuterium exchange mass spectrometry (HDX-MS) coupled with proteolytic digestion provided mechanistic understanding of the intermolecular interactions in the fibrillation of human calcitonin (hCT). The HDX-MS results were used to develop fibrillation-resistant hCT analogs by phosphorylation of specific hCT residues. One such analog, phospho-Thr-13 hCT, showed complete inhibition of fibrillation, whereas others showed partial inhibition. Reduction of the Cys1-Cys7 disulfide bond resulted in faster fibrillation and involvement of different hCT residues. The results demonstrate that pulsed HDX-MS can be used to identify the residues involved in the fibrillation of native and sequence-modified hCT and that site-specific phosphorylation can effectively inhibit fibrillation.

INTRODUCTION

Human calcitonin (hCT) is a 32-amino-acid peptide hormone that plays an important role in skeletal protection and calcium metabolism (1). Calcitonin analogs are used to treat bone diseases such as osteoporosis and Paget's disease as well as certain malignancy-induced hypercalcemias, especially in patients for whom alternative treatments are not suitable (2–6). The clinical application of hCT has been limited, however, in part because of its tendency to form amyloid fibrils in solution (2). Fibrillation can lead

ne

Submitted July 6, 2020, and accepted for publication November 10, 2020.

*Correspondence: topp@purdue.edu

Editor: Elizabeth Komives.

https://doi.org/10.1016/j.bpj.2020.11.009

© 2020 Biophysical Society.

to decreased potency and an increased risk of life-threatening immunogenic side effects (2,7). The more slowly aggregating salmon calcitonin (sCT), which has 50% sequence homology to hCT, is used in clinical settings instead (2,3). Despite greater stability than hCT, sCT therapy has been associated with side effects such as vomiting and anorexia and with immune responses such as resistance and antibody formation, limiting its use in certain patient populations (8–11). Moreover, hCT has shown greater potency than sCT under conditions in which its fibrillation could be controlled (12). Thus, there is an unmet clinical need for a fibrillation-resistant hCT as an alternative to sCT for patients with osteoporosis and Paget's disease (13).

The rational design of fibrillation-resistant hCT analogs requires an understanding of the underlying mechanisms

Renawala et al.

of monomer self-assembly into fibrils, especially during the early stages of fibrillation. Early hCT aggregates have shown a central α -helix, a disulfide-bridged N-terminal loop and random coil C-terminus by NMR spectroscopy (14,15). As fibrillation proceeds, the central region undergoes an α -helix-to- β -strand transition with the N-terminal loop remaining intact (14,15). The C-terminal residues that are closer to the central α -helix become incorporated into the β -strand, resulting in a shorter random coil at the C-terminus (14,15). The structural transition from α -helix to β -strand has been observed at both acidic and neutral pH. However, pH-dependent differences in the orientation of the β -sheets have been reported (15). hCT fibrils are thought to form antiparallel β -sheets at neutral pH 7.5, whereas a mixture of parallel and antiparallel β -sheets is thought to form at acidic pH 3.3, as indicated by solid-state ¹³C NMR spectroscopy (14,15). Transmission electron microscopy images have revealed different morphologies of hCT aggregates formed in acidic and neutral solutions, with long, twisted ribbon-like fibrils at pH 3.3 and short straight fibrils at pH 7.5 (16).

Both hydrophobic and electrostatic interactions are important in the molecular packing and reorientation of early aggregates into mature fibrils (17,18). During nucleation, the side chains of aromatic residues Tyr12, Phe16, and Phe19 in the central region of hCT are thought to align to form the hydrophobic core of the amphiphilic α -helical bundle and subsequently to transition into β -sheets to form the nuclei (17,19). Molecular dynamics (MD) simulations have suggested that the side chains of aromatic residues Phe16 and Phe19 align on the same face of the β sheet structure and engage in π - π stacking interactions that stabilize the antiparallel β -sheet conformation of hCT fibrils at neutral pH (17). The pentapeptide sequence D₁₅FNKF₁₉ forms the core of hCT fibrils and is the shortest hCT fragment capable of forming a fibril (15,20). The D₁₅FNKF₁₉ fragment showed random-coil-to-α-helix-to-βturn transitions leading to fibrillation as measured by circular dichroism (CD) spectroscopy, similar to the transitions involved in the fibrillation of full-length hCT (21). A high-resolution, single-crystal x-ray structure of an iodinated $D_{15}FNKF_{19}$ fragment showed π - π stacking interactions between aromatic side chains of Phe16 in parallel β -sheet conformation similar to those observed in an hCT fragment (9–23) using MD simulations (17,22). The π - π interactions are thought to provide favorable energetic contributions and directionality toward self-assembly of amyloid structures (23). Fibrillation of hCT was faster at neutral pH than at acidic pH, implicating pH-dependent electrostatic interactions (14). hCT contains three charged residues, Asp15, Lys18, and His20, all within the central region (18,24). At neutral pH 7.5, favorable intermolecular electrostatic interactions between Asp15 (-1) and Lys18 (+1), located close to the central Phe residues, determine the antiparallel direction of β -sheet fibrils (18). In contrast, at acidic pH 3.3, repulsive intermolecular electrostatic interactions between Lys18 (+1) and His20 (+1), located at the edge of the central aromatic ring cluster, may disturb the π - π stacking interactions among aromatic Phe residues and lead to the formation of a mixture of parallel and antiparallel β -sheet fibrils because of the lack of a favorable direction for intermolecular associations (18).

The Cys1-Cys7 disulfide bond at the N-terminus of hCT creates a loop. The disulfide-bridged N-terminal loop and the residues in this region are conserved in calcitonins across various species and are believed to be critical for receptor binding, activation, and cAMP response (2,25,26). hCT analogs devoid of the disulfide bond showed weak potency and reduced hypocalcemic activity in rats (27,28). Disulfide bonds are thought to inhibit aggregation by increasing the mechanical strength and reducing the conformational dynamics and entropy of peptides and proteins (29–31). Reduction of disulfide bonds has resulted in rapid fibrillation in therapeutic peptides such as somatostatin, insulin, and amylin because of increased conformational flexibility (32–36). Transmission electron microscopy images showed morphological differences between native and reduced insulin and somatostatin fibrils, and MD simulations have revealed marked differences in the H-bonding networks in fibrils of native and reduced somatostatin (34,35). Slight differences in the conformation of fibrils of disulfide-reduced hCT (rhCT) and native hCT have been identified based on chemical shifts in their NMR spectra (14). In the studies reported here, kinetic and mechanistic differences in the fibrillation of native hCT and disulfide-reduced hCT (rhCT) were examined.

Strategies to improve the therapeutic efficacy of calcitonin have primarily focused on modifications to the amino acid sequence or the development of novel delivery approaches (2). Aromatic residues involved in stabilizing hCT fibrils are likely targets for sequence modifications. A trisubstituted leucine analog of hCT (Y12L, F16L, and F19L hCT) showed a 10-fold increase in hypocalcemic potency in rats relative to native hCT (37). Fibrillation-resistant hCT analogs have been designed by mimicking the more slowly aggregating sCT, replacing select hCT residues with those of sCT (Y12L, N17H, A26N, I27T, and A31T hCT and Y12L, N17H hCT); these analogs showed significantly slower fibrillation while maintaining activity and structural similarity to sCT (38,39). However, these sCTlike analogs may also retain some of the side effects associated with sCT therapy. Conformationally constrained bicyclic hCT analogs have been developed with ∼30–400-fold greater hypocalcemic potency in mice than native hCT, perhaps because of stabilization of the bioactive conformation, although the effects of these structural changes on fibrillation have not been reported (40).

Hydrogen-deuterium exchange with mass spectrometric analysis (HDX-MS) has been used to probe the molecular interactions, leading to the formation of transient intermediates

and mature fibrils of peptides and proteins (41–45). In solution HDX-MS, a peptide or protein is exposed to a deuterium donor, typically deuterium oxide (D₂O), and backbone amide protons are "exchanged" for deuterons. Amide protons involved in hydrogen-bonded secondary structures or buried in a protein's core exchange more slowly than those that are solvent exposed (46). Mass spectrometry (MS) of the deuterated protein is used to measure the number of amide groups that have been exchanged based on the increase in molecular mass, and proteolytic digestion can be used to localize sites of deuteration (47,48). Similarly, in pulsed HDX-MS studies, fibrillating peptides are subjected to a short deuterium-labeling period by exposing the reaction mixture to D_2O (43). As fibrils form, deuteration is hindered by intermolecular interactions in the developing fibrils so that monomeric peptide is deuterated to a greater extent than peptide in oligomeric intermediates or the fully formed fibril (46). When combined with proteolytic digestion, pulsed HDX-MS can identify the regions of the peptide that participate in the early stages of fibrillation based on their differential deuterium exchange rates (43).

In the studies reported here, pulsed HDX-MS and other biophysical methods were used to study the effects of structural modifications on hCT fibrillation. Pulsed HDX-MS of fibrillating hCT showed involvement of the N-terminal and central fragments during the early stages of fibrillation at neutral pH, whereas the C-terminal fragments showed limited participation, even in mature fibrils. The HDX-MS results were used to develop fibrillation-resistant hCT analogs by site-specific phosphorylation of select serine and threonine residues in the hCT sequence. When compared with native hCT, the phosphorylated hCT (phCT) analogs showed modified fibrillation that varied with the phosphorylation site. Reduction of the Cys1-Cys7 disulfide bond resulted in faster fibrillation and involved different hCT residues as indicated by pulsed HDX-MS. Overall, the work demonstrates that small changes in the native structure of hCT can produce marked changes in its fibrillation behavior and that an understanding of the underlying mechanisms can be used to develop fibrillation-resistant hCT analogs.

MATERIALS AND METHODS

Materials

Research-grade hCT and phCT derivatives were purchased from ABclonal Technology (Woburn, MA). hCT had the amino acid sequence C₁GNLSTCMLG₁₀TYTQDFNKFH₂₀TFPQTAIGVG₃₀AP-NH₂, with a Cys1-Cys7 disulfide bond at the N-terminus and amidation at the C-terminus. The three phCT derivatives included phospho-Ser-5 hCT, phospho-Thr-13 hCT, and phospho-Thr-21 hCT, with phosphorylation at respective serine or threonine residues. The peptides had greater than 95% purity, as determined by the manufacturer (see Certificates of Analysis). D2O (99.9%) was purchased from Cambridge Isotope Laboratories (Andover, MA). Thioflavin T (ThioT) was procured from Abcam (Cambridge, MA), and Tris 2-carboxyethyl phosphine (TCEP) hydrochloride was purchased from Sigma-Aldrich (St. Louis, MO). All other chemicals were at least reagent grade and used as received.

Sample preparation

As received, hCT and phCT contained trifluoroacetate salt impurities that were removed by dialysis. The peptides were dissolved in deionized (di)-water at 2 mg/mL and dialyzed using 2-kDa MWCO Slide-A-Lyzer Dialysis Cassettes (Thermo Fisher Scientific, Waltham, MA) with di-water as the dialysis medium (6 h at 4°C, media change every 2 h). The resulting peptide solutions were filtered through a 0.1-\mu m polyvinylidene difluoride (PVDF) filter and transferred to lyophilization vials (size 2R; DWK Life Sciences, Millville, NJ), then freeze dried using a pilot-scale LyoStar 3 lyophilizer (SP Scientific, Warminster, PA) to obtain dried and purified peptide powder, which was then stored at -80° C until use. rhCT was produced from hCT using TCEP. Briefly, hCT was dissolved in di-water at 2 mg/mL, and a 100-mM TCEP stock solution was added to give a final TCEP concentration of 5 mM. The solution was allowed to stand for 15 min at 25°C to complete the reduction, then dialyzed to remove dissolved salt impurities and TCEP. The solution was lyophilized to obtain dried and purified rhCT as above.

Fibrillation kinetics by ThioT fluorescence and turbidity measurements

The fibrillation kinetics of hCT, rhCT, and phCT was monitored in 96-well plates using a Synergy Neo2 Multi-Detection Microplate Reader (BioTek Instruments, Winooski, VT). ThioT fluorescence and turbidity were monitored under the same conditions. ThioT is a fluorescent dye that shows increased fluorescence on binding to the hydrophobic pockets of β -sheetrich fibrils (49,50). In ThioT studies, peptides (100 μ M, \sim 0.34 mg/mL) were dissolved in cold 20 mM sodium phosphate buffer (pH 7.4) and quickly transferred to a 96-well microtiter plate. In each well, 5 μ L of ThioT working solution (250 μ M) was added to 245 μ L of peptide solution to give a final ThioT concentration of 5 µM per well. Fibrillation was allowed to proceed for 12 or 24 h at 25°C, with continuous shaking at 731 cpm. Fluorescence intensity was bottom read every 10 or 15 min at excitation and emission wavelengths of 440 and 482 nm, respectively. Six replicate measurements were performed for each time point. The resulting ThioT data were fitted to the Boltzmann sigmoidal function (Eq. 1) using GraphPad Prism version 7.04 (GraphPad Software, La Jolla, CA):

$$Y = A_1 + \frac{A_2 - A_1}{1 + e^{(x_0 - x)/dx'}},\tag{1}$$

where A_1 is the minimal signal, A_2 is the maximal signal, x_0 is the time at which the change in signal is 50% (t_{50}) and dx' is the slope of the growth phase (43). The fibrillation lag time was determined as $x_o - 2dx'$ using the regression parameters. For data that did not fit satisfactorily to Eq. 1, the lag time was determined from the intersection of tangents to the lag phase and growth phase curves (51). Lag times determined from Eq. 1 and from tangent methods were within 3% of one another. Similarly, when data did not fit Eq. 1 satisfactorily, the fibrillation half-life (t50) was estimated as the time when the signal intensity reached half the maximal value.

Fibrillation kinetics were also monitored by measuring solution turbidity. Samples were prepared and the studies performed as above but without added ThioT. Turbidity was measured by ultraviolet (UV) absorbance at 340 nm at 10- or 15-min read intervals, and six replicate measurements were performed. Turbidity data were fitted to the Boltzmann sigmoidal function (Eq. 1) and analyzed as above.

CD spectroscopy

Changes in peptide secondary structure during fibrillation were monitored by CD spectroscopy using a Jasco J-815 spectrometer (JASCO Analytical Instruments, Easton, MD). Solution samples were prepared as for turbidity measurements and allowed to fibrillate in 96-well microtiter plates in the plate reader. At predetermined time intervals, samples were withdrawn, Please cite this article in press as: Renawala et al., Fibrillation of Human Calcitonin and Its Analogs: Effects of Phosphorylation and Disulfide Reduction, Biophysical Journal (2021), https://doi.org/10.1016/j.bpj.2020.11.009

Renawala et al.

and CD spectra were recorded in a quartz cuvette with a 1-mm pathlength scanned from 190 to 260 nm in the far-UV range at a scan speed of 50 nm/min at 20° C. Spectra are reported as an average of three scans.

Pulsed amide HDX-MS

In pulsed HDX-MS studies of fibrillating peptides, samples were prepared and allowed to fibrillate in 96-well plates in the microplate reader as described above. At predetermined time intervals (0–1440 min), triplicate samples were withdrawn and subjected to pulsed deuteration. The sampling time was negligible (\sim 1 min) compared with the overall fibrillation time course. For rhCT, because fibrillation was rapid, sampling times were divided among three independent experiments. For all peptides, a 2-min pulse deuterium-labeling period was initiated by diluting a 5- μ L sample of fibrillating peptide in 45 μ L of D₂O (99.9%), resulting in a final concentration of 90% D₂O (v/v) and 10 μ M peptide. At the end of the labeling period, the exchange was quenched by adding 45 μ L of ice-cold quench buffer (5% w/v urea, 5% v/v methanol, and 0.2% v/v formic acid (FA) in MS grade water (pH 2.5)). Quenched samples were flash frozen in liquid nitrogen and stored at -80° C until analysis.

As a control, the rate and extent of deuterium uptake were measured for hCT under conditions when fibrillation did not occur. A 100- μ M (\sim 0.34 mg/mL) hCT solution was prepared in 20 mM sodium phosphate buffer (pH 7.4) at room temperature. Deuteration was initiated by 10-fold dilution of the hCT solution with D₂O (99.9%) to a final concentration of \sim 90% D₂O (v/v) and 10 μ M hCT. The solution was kept undisturbed at room temperature for 120 min. Aliquots of 45 μ L were withdrawn at various times, quenched, flash frozen, and stored until analysis as above.

Deuterium uptake was measured using a liquid chromatography mass spectrometry (LC-MS) system (Agilent 6520 QTOF; Agilent Technologies, Santa Clara, CA) equipped with a custom-built refrigeration unit that maintained the LC column at low temperature (~2°C) to minimize back exchange. Deuterated samples were quickly thawed, and ~250 pmol of peptide was injected into the LC-MS system. Samples were retained on a peptide microtrap (Michrom Bioresources, Auburn, CA) and desalted (0.1% FA in water, 1.7 min, 0.2 mL/min). The peptide was then eluted in 4.5 min onto an analytical column (Zorbax 300SB-C18; Agilent Technologies) using a gradient of acetonitrile (25-59%), water, and 0.1% FA at a flow rate of 50 µL/min. Mass spectra were collected over the m/z range of 100-1700. To measure deuterium uptake at the fragment level, samples were subjected to proteolytic digestion by injecting them into an in-line immobilized pepsin column maintained at 25°C within the refrigeration unit. Online digestion was carried out for 1.7 min in water containing 0.1% FA at a flow rate of 0.2 mL/min. The fragments were retained on a peptide microtrap, desalted, and then eluted onto a C18 analytical column as above.

For HDX-MS at the fragment level, a list of peptide fragments was generated from each undeuterated control using MassHunter Workstation software equipped with the Bioconfirm software package (B.03.01; Agilent Technologies). Peptides identified using undeuterated controls were mapped onto deuterated samples using HDExaminer software (Version 2.0; Sierra Analytics, Modesto, CA). For fibrillating peptides with a bimodal distribution of deuterium uptake, the percent of deuteration was calculated as a weighted average of the two populations. Deuterium uptake values were not subjected to back exchange correction, and all values are reported as the mean of three independent hydrogen-deuterium exchange (HDX) experiments. Additional details on the HDX-MS experiments are provided in Data S1 using the format suggested by Masson et al. (52).

For the controls, the extent of deuteration as a function of time was fitted to a monoexponential association model (Eq. 2):

$$D = D_{max} \left(1 - e^{-kt} \right), \tag{2}$$

where D_{max} is the maximal deuteration, k is the exchange rate constant, and t is deuteration time (in minutes). Deuterium uptake data for fibrillating hCT were fitted to the Boltzmann sigmoidal function (Eq. 1). For fibrillating

rhCT, deuterium uptake data were fitted to a monoexponential decay model (Eq. 3):

$$D = (D_0 - D_{\infty})e^{-kt} + D_{\infty}, \tag{3}$$

where D_0 is the deuterium uptake at time t=0 of fibrillation, D_{∞} is the deuterium uptake at large fibrillation times, k is the exchange rate constant, and t is deuteration time (in minutes). Data analysis was performed using GraphPad Prism version 7.04.

RESULTS

Fibrillation kinetics using fluorescence and turbidity measurements

During fibrillation, an increase in ThioT fluorescence was observed for both hCT and rhCT, consistent with the formation of β -sheet-rich fibrils (Fig. 1). An increase in turbidity was also observed, consistent with an increase in the number and/or size of particles (Fig. 1). For both ThioT and turbidity measurements, fibrillation kinetics showed sigmoidal behavior, with lag, growth, and equilibrium phases characteristic of a nucleation-dependent aggregation process (51). For hCT, there was no significant difference in fibrillation lag times measured by the two methods (Table 1). Under similar conditions, the fibrillation of rhCT was significantly faster than that of hCT, with shorter lag time and t₅₀-values (Fig. 1; Table 1). For rhCT, the t₅₀-value by ThioT fluorescence was $\sim 2 \times$ greater than the t_{50} -value by turbidity (Table 1), suggesting that particles were present before ThioT intercalation occurred. The changes in the secondary structure of hCT and rhCT during fibrillation, as detected by CD spectroscopy, coincided with the changes observed by ThioT and turbidity measurements (Figs. 1 and S1). CD spectra of fibrillating hCT and rhCT showed a loss of negative intensity with time, consistent with a loss of random coil conformation and the formation of insoluble fibrils (Fig. S1).

Amide HDX-MS

HDX-MS for monomeric hCT

HDX-MS was performed for monomeric hCT at both intact and fragment levels to serve as a control for pulsed deuteration studies of fibrillating hCT. At the intact level, deuterium uptake for monomeric hCT reached 82% of the theoretical maximum after 20 min (Fig. S2 A), suggesting an upper limit for back exchange of ~18% in this system in agreement with previous HDX-MS studies of unstructured peptides in our lab (53). After deuteration, intact mass spectra showed a single peak consistent with a single population of monomeric hCT (Fig. S3). After pepsin digestion, a total of six fragments were selected having strong and reproducible MS signals and providing 100% sequence coverage with some overlap (Fig. S2 B). The six fragments reached similar maximal deuterium uptake (59–66% of

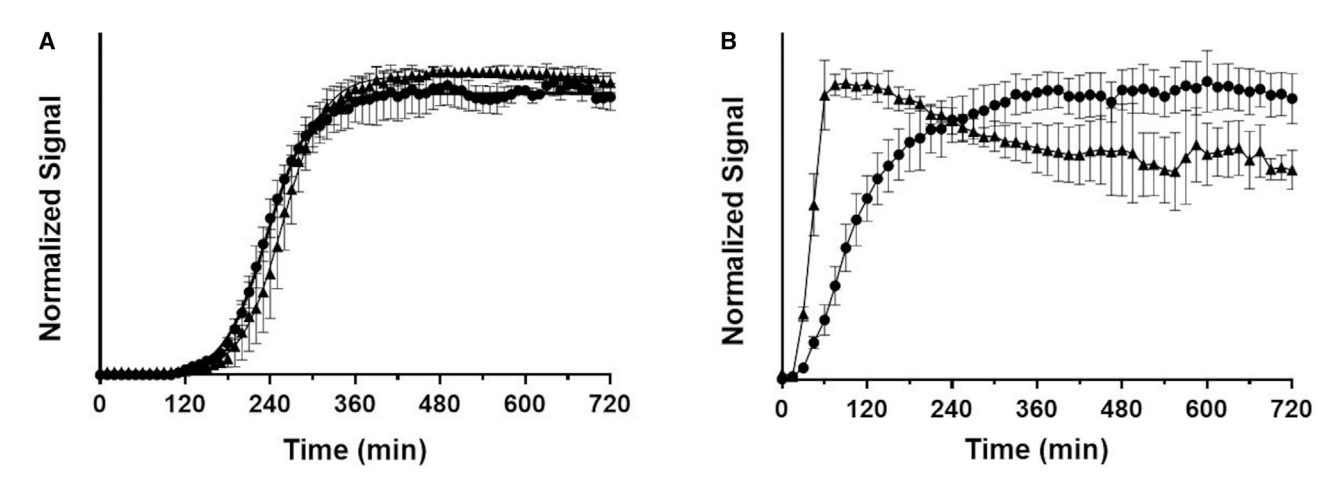


FIGURE 1 Fibrillation kinetics of human calcitonin (hCT) (A) and reduced hCT (rhCT) (B) by ThioT fluorescence (solid circles) and turbidity (solid triangles) measurements. The hCT and rhCT were dissolved in 20 mM sodium phosphate buffer (pH 7.4) at 100 µM and allowed to fibrillate at 25°C with continuous shaking at 731 cpm in a 96-well microtiter plate. n = 6, mean \pm standard deviation (SD).

theoretical maximum) in less than 2 min of D₂O exposure, indicating dynamic flexibility and limited higher order structure (Fig. S2 B).

HDX-MS for fibrillating hCT at intact level

At the initiation of the fibrillation experiment (t = 0 min), hCT showed a single mass envelope with little peak broadening relative to the undeuterated control (Fig. 2 A). This peak (peak II) corresponds to hCT that is highly solvent exposed and deuterated at the level measured under monomeric conditions (%D = 68). Similar envelopes were observed until 100 min of fibrillation (Fig. 2 A), corresponding with the lag phase measured in ThioT and turbidity studies (Fig. 2 B). After 100 min of fibrillation, a new peak (peak I) was observed, with lower m/z indicating greater protection from exchange and consistent with the presence of hCT oligomers or proto fibrils (Fig. 2 A). As fibrillation proceeded, the intensity of peak I increased, and the intensity of peak II decreased, with an overall reduction in deuteration levels (Fig. 2, A and B). At 360 min, peak II appeared as a shoulder, suggesting a near-complete shift in population from monomeric to oligomeric hCT. After

TABLE 1 Fibrillation Kinetic Parameters (t₅₀ and Lag Time) of hCT and rhCT as Determined by ThioT Fluorescence, Turbidity, and HDX-MS Measurements

Measurement	Parameter (min)	hCT	rhCT
ThioT fluorescence ^a	t ₅₀	236 ± 8	113 ± 16
	lag time	172 ± 15	34 ± 9
Turbidity ^a	t ₅₀	257 ± 15	50 ± 8
	lag time	198 ± 20	23 ± 6
HDX-MS ^b (intact level)	t ₅₀	165 ± 7	46 ± 7
	lag time	104 ± 7	NA

NA, not applicable; mean \pm SD.

1440 min of fibrillation, the percent of deuterium uptake was 28%, suggesting that some solvent-accessible regions remain in these more mature hCT fibrils (Fig. 2 A).

The deuterium uptake at any time is the weighted average of the number of deuterons in both the protected and solvent-accessible populations and was fitted to a Boltzmann sigmoid function (Eq. 1; Fig. 2 B). The lag time of fibrillation by HDX-MS was significantly shorter than for ThioT and turbidity measurements, in agreement with the detection of a more protected population (peak I) at 100 min by HDX-MS (Fig. 2 A; Table 1). A significantly shorter t₅₀value was observed for HDX-MS than for ThioT or turbidity measurements (Table 1). This suggests that the intermolecular interactions and structural changes detected by HDX-MS precede those detected by the other methods (Table 1) and that the peptide may be fully protected from exchange before rearranging into fibrils that can bind ThioT and increase solution turbidity.

HDX-MS for fibrillating hCT at fragment level

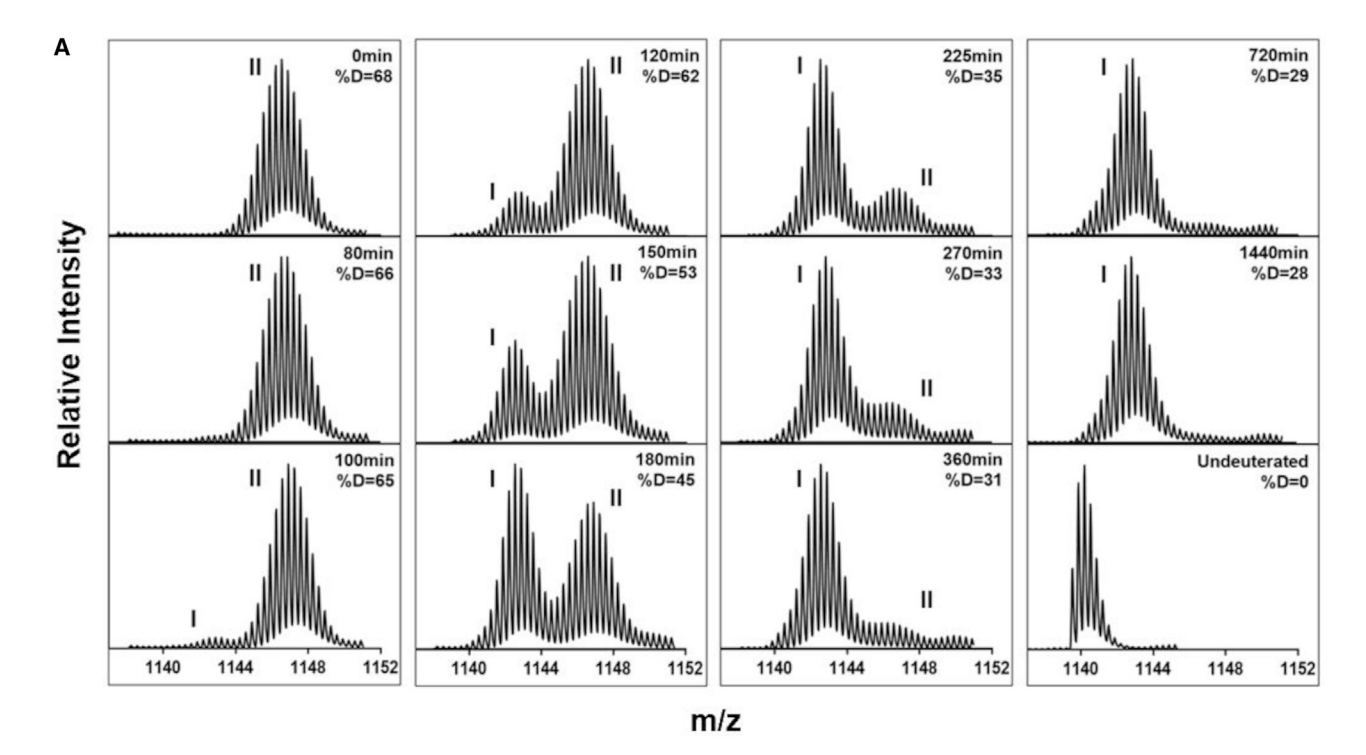
Fibrillating hCT was subjected to HDX-MS with pepsin digestion to identify the regions that show protection from deuteration during the early stages of fibril formation. Deuterium uptake of six hCT fragments was monitored, providing 100% sequence coverage with some overlap (Fig. 3 A). The average mass of native hCT (3418.1004 g/ mol), as measured by MS, indicated that the Cys1-Cys7 disulfide bond at the N-terminus remained intact during fibrillation and MS analysis. During the initial 100 min of fibrillation, no significant change was observed in the deuteration of the fragments (Fig. 3 A), consistent with HDX results at the intact level (Fig. 2 B). After 100 min, the rate and extent of deuterium uptake varied among fragments from different regions. Overlapping fragments 1-8 and 1–11, from the N-terminus, and the central fragment 12-19 all showed a decrease in deuterium uptake with

 $^{^{}a}n = 6$

 $^{^{\}rm b} n = 3$

Please cite this article in press as: Renawala et al., Fibrillation of Human Calcitonin and Its Analogs: Effects of Phosphorylation and Disulfide Reduction, Biophysical Journal (2021), https://doi.org/10.1016/j.bpj.2020.11.009

Renawala et al.



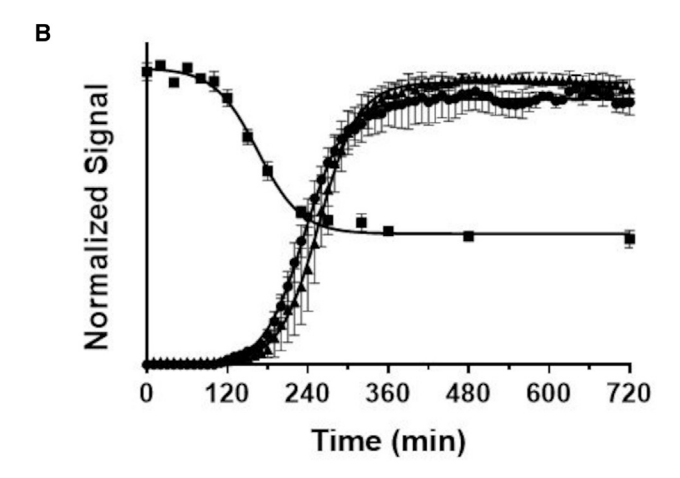


FIGURE 2 Pulsed HDX-MS of fibrillating hCT at intact level. The fibrillating hCT was pulse labeled with deuterium for 2 min at intervals over the fibrillation time course (to 1440 min) and analyzed for deuterium uptake by MS. (A) Shown is the enhanced mass envelope of deuterated and undeuterated hCT (m/z = 1139.5416; z = +3) at the intact level. The spectra show a bimodal peak distribution (peaks I and II) during fibrillation. %D is the average percent of deuterium uptake by hCT (n = 3). (B) Shown is the fibrillation kinetics of hCT by ThioT fluorescence (solid circles; n = 6), turbidity (solid triangles; n = 6), and deuterium uptake by HDX-MS at the intact level (solid squares; n = 3). Lines are fits to Boltzmann sigmoid function (Eq. 1). Mean \pm SD.

fibrillation time. This decrease was significantly greater than in fragments 20-32 and 26-32 from the C-terminus (Figs. 3 A and S4). After 1440 min, deuterated mass envelopes of the N-terminal (1–8 and 1–11) and central (12–19) fragments showed a near-complete shift toward a more protected population, whereas the C-terminal fragments (20–32 and 26– 32) only showed minor peak broadening (Fig. S4). Fragment 16–28, which contains overlapping residues from fragments 12–19 and 20–32, showed intermediate behavior (Figs. 3 A and \$4).

The deuteration kinetics for fragments 1–8, 1–11, and 12– 19 was fitted to a Boltzmann sigmoid function (Eq. 1). This analysis was not applied to fragments 16-28, 20-32, and 26–32, which showed a small overall change in deuterium uptake (Fig. 3 A). The half-lives of deuterium uptake for fragments 1–8, 1–11, and 12–19 did not show significant differences (Fig. 3 B). For the N-terminal (1–11) and central (12–19) regions, both the relatively rapid decrease in deuterium incorporation and the significant decrease in deuteration after 360 min suggest that this region is involved in

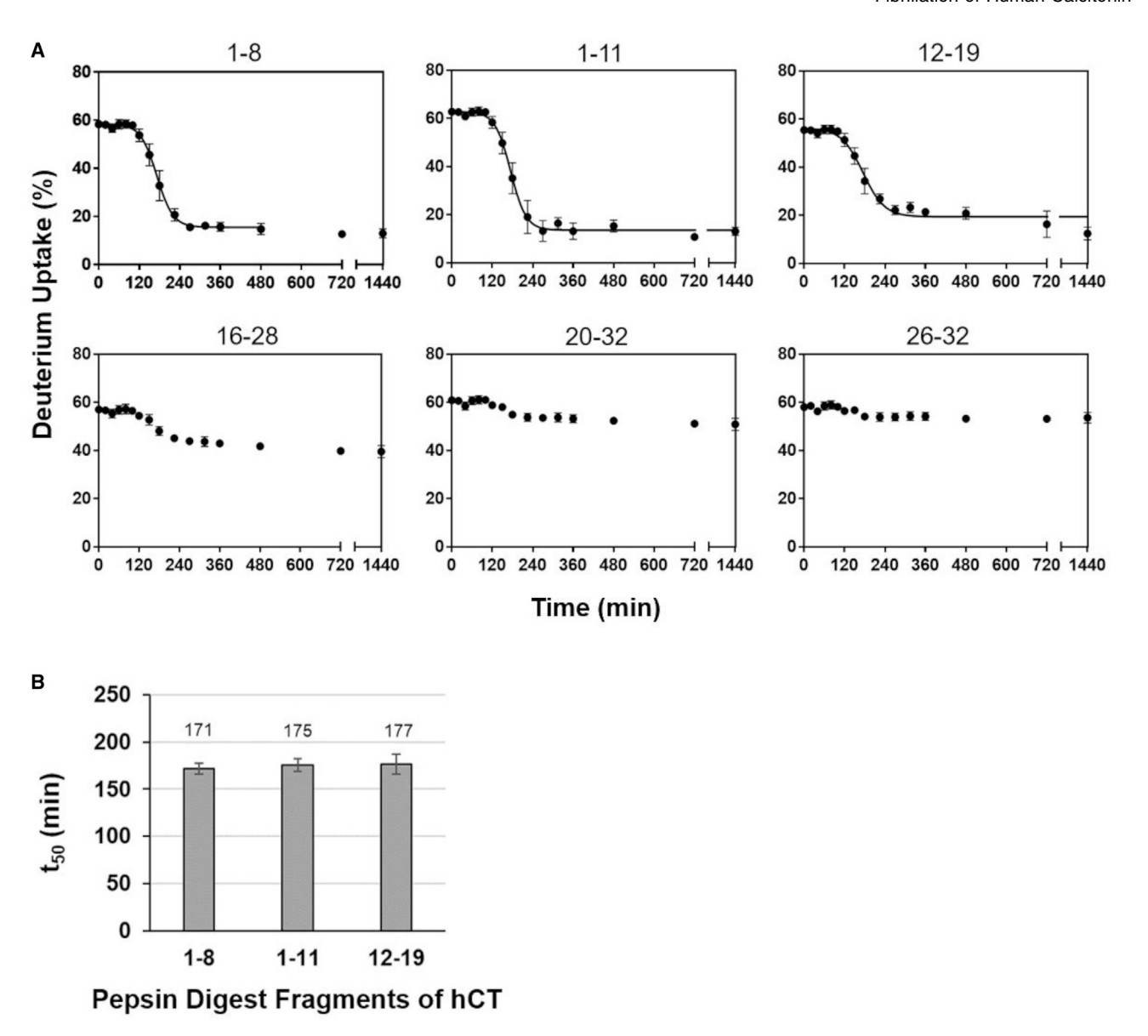


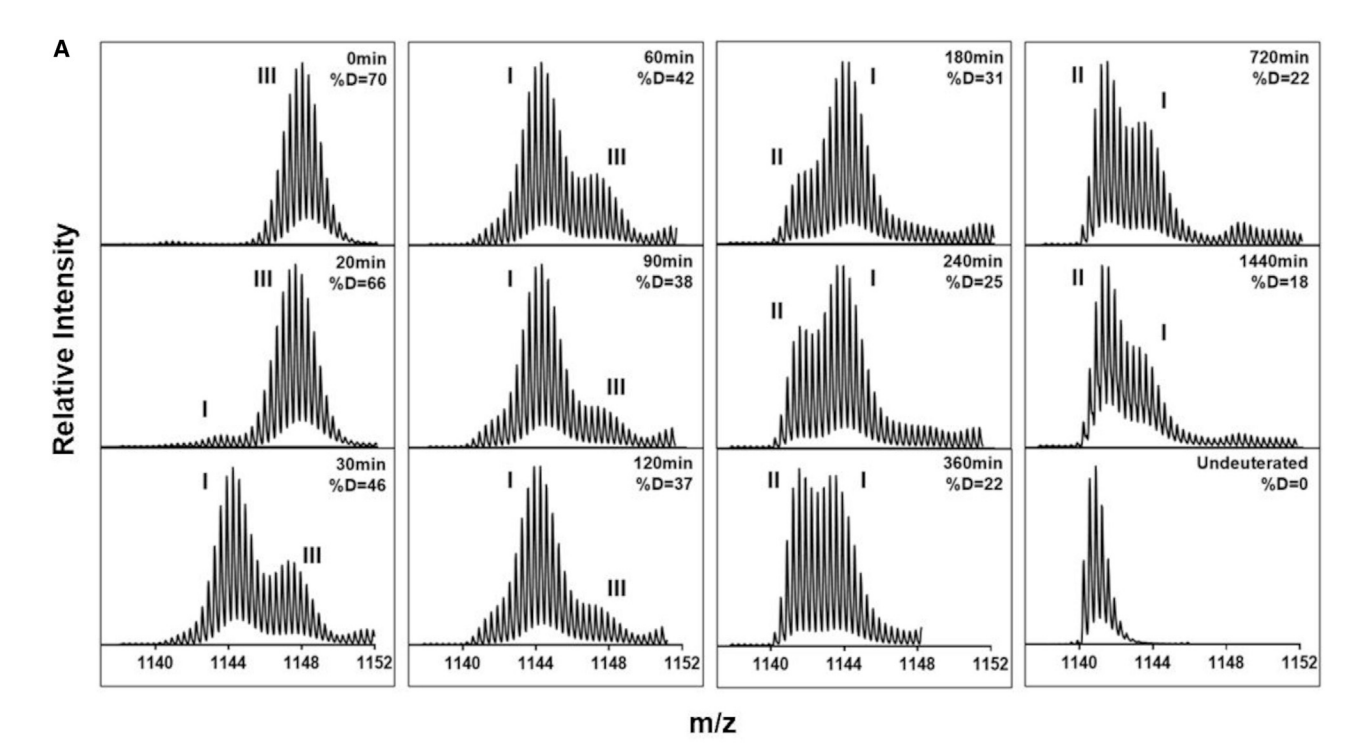
FIGURE 3 Pulsed HDX-MS of fibrillating hCT at the fragment level. The fibrillating hCT was pulse labeled with deuterium for 2 min at intervals over the fibrillation time course (to 1440 min) and analyzed for deuterium uptake by MS after pepsin digestion. (A) Shown is the percent of deuterium uptake for the hCT fragments 1-8, 1-11, 12-19, 16-28, 20-32, and 26-32 as a function of time of fibrillation. The lines represent fit to Boltzmann sigmoid function (Eq. 1) in cases in which good fit was achieved (n = 3, mean \pm SD). (B) Shown are the t_{50} -values for deuterium incorporation in three hCT fragments (n = 3, mean \pm SD).

the early stages of hCT fibrillation (Fig. 3 A). In contrast, for the C-terminal region (20-32 and 26-32), the relatively slow and limited decrease in deuterium incorporation, even after 1440 min (Fig. 3 A), suggest that this region does not participate directly in fibril growth and maturation under these conditions.

HDX-MS for fibrillating rhCT at intact level

The Cys1-Cys7 disulfide bond in native hCT was reduced using TCEP to study the effects of reduction on fibrillation kinetics. During fibrillation of rhCT, the initial (t = 0 min)deuterated mass envelope appeared as a single peak, with little peak broadening relative to the undeuterated control (Fig. 4 A). This unimodal peak (peak III) corresponds to monomeric rhCT and showed maximal deuterium uptake of 70% (Fig. 4 A). After 20 min of fibrillation, a more protected population (peak I) emerged at lower m/z (Fig. 4 A). By 30 min, the intensity of peak I had increased markedly, with a corresponding decrease in the intensity of peak III. During the same time interval, the percent deuterium incorporation decreased from 66% at 20 min to 46% at 30 min, which corresponded to an increase in ThioT and turbidity signals (Fig. 4, A and B). From 30 to 120 min, peak I increased somewhat more slowly, in contrast to its earlier Please cite this article in press as: Renawala et al., Fibrillation of Human Calcitonin and Its Analogs: Effects of Phosphorylation and Disulfide Reduction, Biophysical Journal (2021), https://doi.org/10.1016/j.bpj.2020.11.009

Renawala et al.



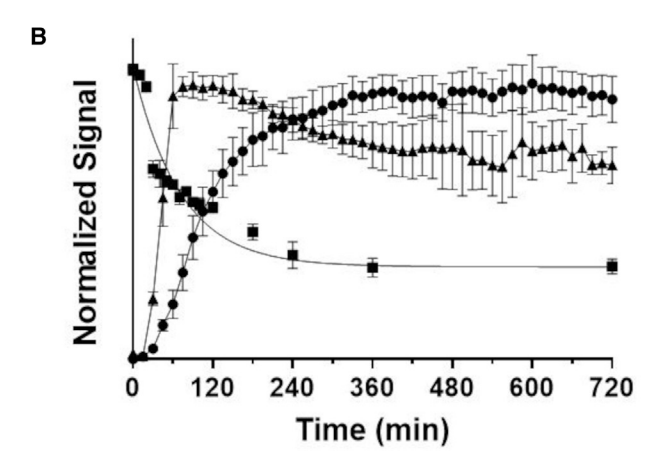


FIGURE 4 Pulsed HDX-MS of fibrillating reduced rhCT at intact level. The fibrillating rhCT was pulse labeled with deuterium for 2 min at intervals over the fibrillation time course (to 1440 min) and analyzed for deuterium uptake by MS. (A) Shown are the enhanced mass envelopes of deuterated and undeuterated rhCT (m/z = 1140.2375; z = +3) at the intact level. The spectra show a bimodal peak distribution (peaks I and II and peaks I and III) during fibrillation. %D is the average percent of deuterium uptake by rhCT (n = 3). (B) Shown is the fibrillation of the rhCT by ThioT fluorescence (solid circles; n = 6), turbidity (solid triangles; n = 6), and deuterium uptake by HDX-MS (solid squares; n = 3). The HDX data are fitted to a monoexponential decay model (Eq. 3). Lines show trends for ThioT fluorescence and turbidity measurements and do not represent regression. Mean ± SD.

rapid growth (Fig. 4 A). At 120 min, there was a slight broadening of peak I at lower m/z, whereas peak III diminished to a shoulder (Fig. 4 A). By 180 min, a second protected population appeared (peak II), which was more protected from deuteration and had lower m/z than peak I, and peak III completely disappeared (Fig. 4 A). With further fibrillation, the intensity of peak II increased gradually with a corresponding decrease in the intensity of peak I, accompanied by a gradual decrease in percent deuterium uptake from 31 to 18% between 180 and 1440 min (Fig. 4, A and B). Deuterium incorporation at 1440 min was less for rhCT (18%) than for hCT (28%) (Figs. 2 and 4), suggesting that a greater portion of the rhCT sequence is incorporated in the mature fibrils.

Deuterium uptake was plotted as a function of fibrillation time and fitted to a monoexponential decay model (Eq. 3; Fig. 4 B). The fibrillation half-life (t_{50}) of rhCT is significantly shorter for HDX-MS than for ThioT but similar to that for the turbidity measurement (Table 1), suggesting that the structural changes detected by HDX-MS coincide with the detection of

particles by turbidity measurement but precede the formation of ThioT-intercalating fibrils for rhCT.

Under quiescent conditions, the free sulfhydryl (-SH) groups in rhCT monomers were stable against oxidation over 24 h at room temperature, as indicated by the absence of a peak in the mass spectrum corresponding to native hCT after incubating rhCT for 24 h without shaking (Fig. S5). Additional evidence for the oxidative stability of rhCT during fibrillation is provided by the digest data for fragment 1-8, which contains both of the Cys residues (Cys1 and Cys7) that participate in the disulfide bond. Fragment 1-8 shows different fibrillation kinetics in hCT and rhCT (see Figs. 3 A and 5 A) and has different deuterated masses when fully fibrillated (see Figs. S4 and S6), suggesting that the fragment is chemically different in the two peptides throughout the fibrillation time course.

HDX-MS for fibrillating rhCT at fragment level

To identify the regions of the rhCT sequence that are protected from exchange during fibrillation, samples were subjected to proteolytic digestion before MS analysis. A total of six fragments were identified that provided 100% sequence coverage with some overlap. During fibrillation, a decrease in deuterium uptake was observed for all rhCT fragments (Fig. 5 A). Fragments from different regions of the rhCT sequence showed greater differences in deuteration during the first 120 min than at later times (Fig. 5 A). From t = 0 to 120 min, the percent of deuterium incorporation in the central fragments 9-15 and 12-19 decreased rapidly, whereas the C-terminal fragments 20-32 and 26-32 showed little change (Fig. 5 A). At 120 min, the deuterated mass envelopes of fragments 9-15 and 12–19 showed a near-complete shift toward a single

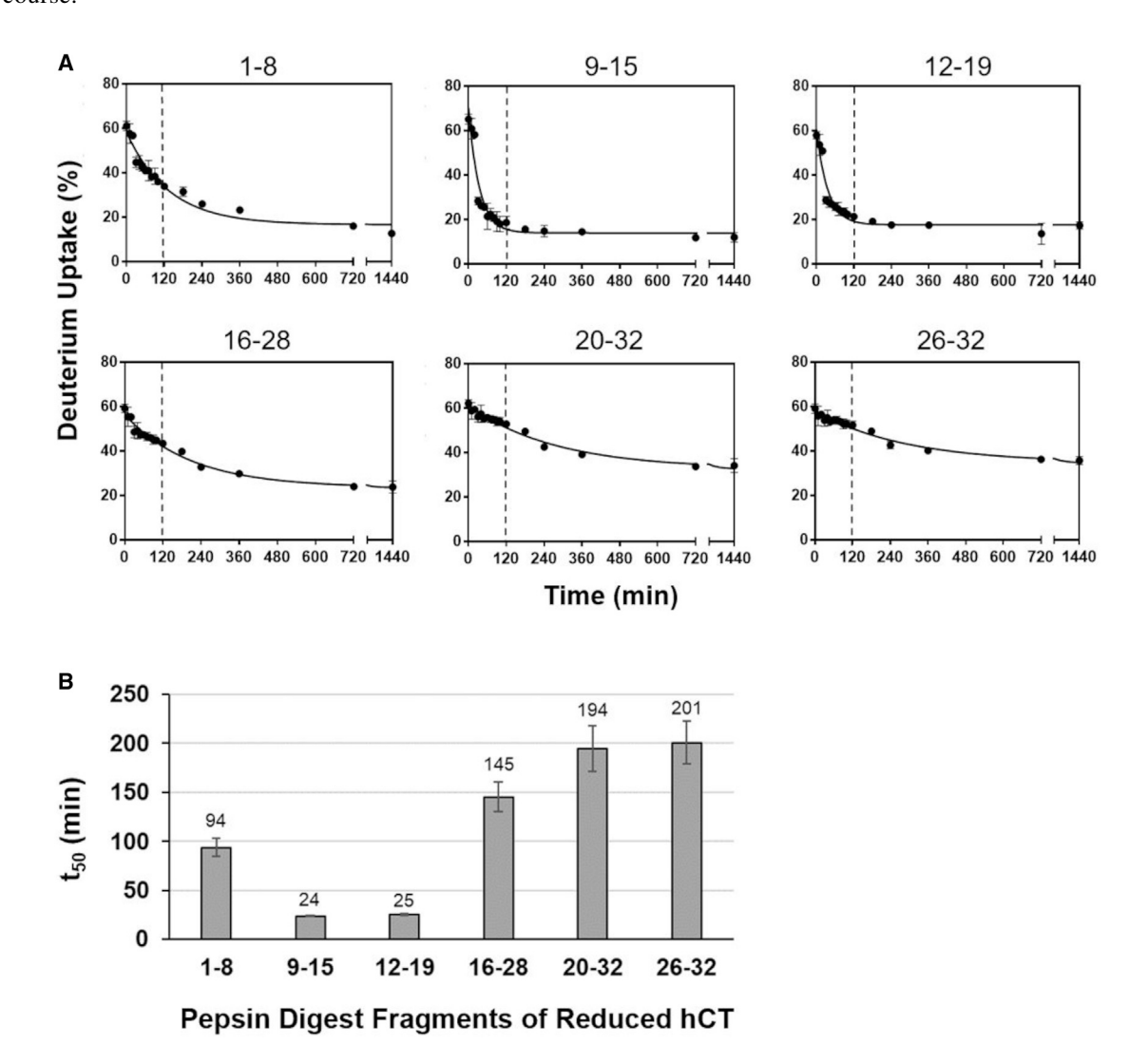


FIGURE 5 Pulsed HDX-MS of fibrillating rhCT at the fragment level. The fibrillating rhCT was pulse labeled with deuterium for 2 min at intervals over the fibrillation time course (to 1440 min) and analyzed for deuterium uptake by MS after pepsin digestion. (A) The percent of deuterium uptake for the rhCT fragments 1-8, 9-15, 12-19, 16-28, 20-32, and 26-32 as a function of time of fibrillation. Lines represent fits to monoexponential decay model (Eq. 3) (n=3, mean \pm SD). (B) Shown are the t₅₀-values for deuterium incorporation in six rhCT fragments (n = 3, mean \pm SD).

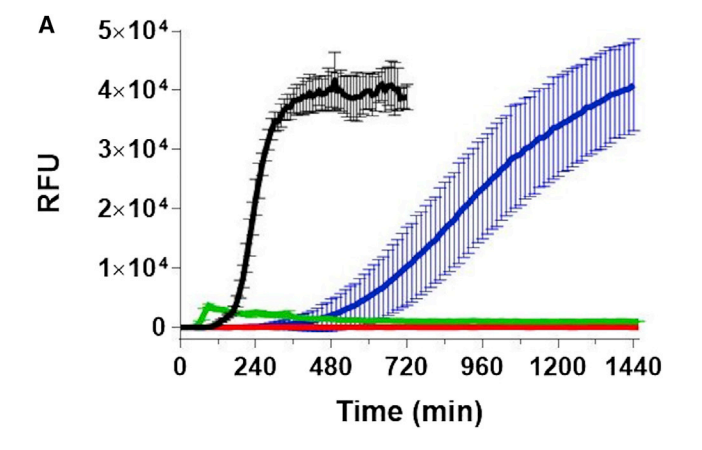
Renawala et al.

protected population, whereas the mass envelopes of fragments 20–32 and 26–32 showed little change (Fig. S6). The N-terminal fragment 1–8 showed a slower decrease in deuterium uptake than the central region (9–15 and 12–19) from 0 to 120 min, but a faster decrease than the C-terminal region (16–28, 20–32, and 26–32) (Fig. 5 A). At 1440 min, the deuterated mass envelopes of fragments 16–28 and 20–32 showed bimodal distributions with both protected and unprotected populations, whereas fragments 1–8, 9–15, and 12–19 showed only a single population (Fig. S6). Fragment 16–28, which contains overlapping residues from fragments 12–19 and 20–32, showed intermediate behavior (Figs. 5 A and S6).

The deuteration kinetics for rhCT fragments were fitted to a monoexponential decay model (Eq. 3). The half-life (t_{50}) of deuterium uptake for the C-terminal fragments (20-32 and 26–32) was $\sim 8 \times$ greater than values for the central region fragments (9–15 and 12–19) and \sim 2× greater than the N-terminal fragment (1–8) (Fig. 5 B). For the central region (9–19), the relatively rapid decrease in deuterium incorporation and the near-complete shift to a more protected population at 120 min suggest that this region participates in the early stages of fibrillation (Figs. 5 A and S6). The slower decrease in deuterium incorporation near the C-terminus suggests that this region participates at later stages of fibril growth and maturation (Fig. 5 A). The presence of both protected and accessible populations and the relatively high deuterium incorporation at 1440 min suggest that the C-terminus is more exposed in the mature fibrils than the central region (Fig. S6). For the N-terminus (1–8), the slower decrease in deuterium incorporation relative to the central region (Fig. 5 A) and a gradual but complete shift to a more protected population with lower percent deuterium incorporation at 1440 min (Fig. S6) suggest that this region is incorporated into the fibrillar structure after the central region.

Fibrillation kinetics of phCT derivatives

Three phCT derivatives were monitored for fibrillation under stressed conditions by ThioT fluorescence and turbidity measurements (Fig. 6). The derivatives showed differences in fibrillation behavior that depended on the site of phosphorylation. An increase in ThioT fluorescence with time was observed for both phospho-Ser-5 hCT and phospho-Thr-21 hCT, consistent with the formation of fibrils (Fig. 6 A). Phospho-Thr-13 hCT did not show a change in ThioT fluorescence under these conditions, suggesting that fibrillation had been inhibited (Fig. 6 A). Although the lag time of fibrillation by ThioT was shorter for phospho-Ser-5 hCT (lag time = $58 \pm 8 \text{ min}$) than for native hCT (lag time = $172 \pm 8 \text{ min}$) 15 min), the ThioT signal intensity was \sim 10-fold weaker for phospho-Ser-5 hCT than for native hCT (Fig. 6 A; Table S1). The lower ThioT signal intensity for phospho-Ser-5 hCT suggests the formation of oligomeric intermediates and/or protofibrils, which interact more weakly with ThioT than mature fibrils (54). Phospho-Thr-21 hCT showed a much greater fibrillation lag time (lag time = 568 ± 95 min) but similar ThioT signal intensity compared with native hCT (Fig. 6 A; Table S1). The growth of fibrils in phospho-Thr-21 hCT did not plateau in 24 h, as observed by ThioT fluorescence (Fig. 6 A). Turbidity measurements for phospho-Ser-5 hCT showed a significantly lower signal intensity (Fig. 6 B); on visual inspection, a thin translucent film was observed at the bottom of the 96-well plates after 24 h. In contrast, solid dense deposits were observed for hCT and rhCT fibrillation. There were no significant changes in turbidity for phospho-Thr-13 or phospho-Thr-21 hCT, and both solutions remained clear on visual inspection (Fig. 6 B). Phospho-Thr-13 hCT, when subjected to more aggressive fibrillation conditions (25°C, continuous shaking at 1096 cpm) for 840 min, showed no change in ThioT or turbidity signals (Fig. S7).



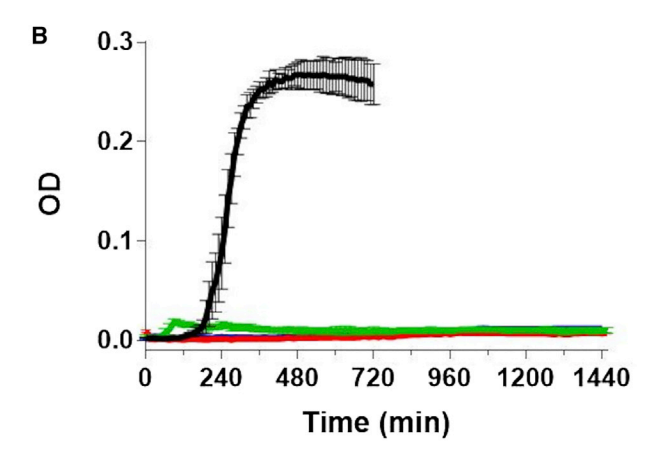


FIGURE 6 Effect of site-specific phosphorylation on the fibrillation of three phosphorylated hCT (phCT) derivatives: phospho-Ser-5 hCT (green), phospho-Thr-13 hCT (red), and phospho-Thr-21 hCT (blue) compared with hCT control (black). The fibrillation was monitored by ThioT florescence (RFU) at 482 nm (A) and turbidity (OD) at 340 nm (B) under fibrillation conditions (100 μ M peptide in 20 mM sodium phosphate buffer (pH 7.4) at 25°C, with continuous shaking at 731 cpm for 12–24 h in a 96-well microtiter plate). n=6, mean \pm SD. To see this figure in color, go online.

These observations were consistent with the changes in secondary structure of the three phCT analogs detected by CD spectroscopy (Fig. S8). Like native hCT, phCT derivatives initially showed CD spectra consistent with a random coil conformation (Fig. S8). Both phospho-Ser-5 hCT and phospho-Thr-21 hCT showed significant reduction in the random coil signal by 1440 min (Fig. S8, A and C), consistent with a loss in free monomer concentration, whereas there was no loss of CD signal for phospho-Thr-13 hCT, which showed nearly identical spectra at 0 and 1440 min (Fig. S8 B).

Stability of phospho-Thr-13 hCT by amide HDX-MS

HDX-MS at the intact level was performed for phospho-Thr-13 hCT samples stressed under fibrillating conditions (25°C, continuous shaking at 731 cpm for 1440 min). At t = 0 min, a single deuterated mass envelope was observed consistent with monomeric phospho-Thr-13 hCT (Fig. S9). No peak broadening or change in peak position was observed after 1440 min (Fig. S9). Deuterium uptake did not change significantly, and the mass spectrum at 1440 min was consistent with monomeric phospho-Thr-13 hCT (Fig. S9), indicating the absence of oligomers or fibrillar intermediates.

DISCUSSION

Amyloid fibrils are formed by the stacking of β -sheets that interact side by side through interdigitation of amino acid side chains to form steric zippers (55). These interactions are mostly noncovalent, mediated through hydrogen bonding, steric or hydrophobic interactions, and/or charge interactions (56). Modifying amino acid side chains through site-specific phosphorylation of hCT interferes with the interactions responsible for steric zipper formation in the core of hCT fibrils. At neutral pH, phosphorylation introduces negative charge (-2) into the zipper-forming side chains, inhibiting monomer self-association through charge repulsion. HDX-MS results for fibrillating hCT implicate the N-terminal (1– 11) and central (12–19) regions in the early stages of fibrillation, whereas the C-terminal (20-32) region had limited involvement (Figs. 3 A and S4). Based on these findings, three phCT derivatives were selected to probe the effects of phosphorylation site on fibrillation. Serine and threonine residues in the disulfide-bridged N-terminal loop (phospho-Ser-5 hCT), in the central region (phospho-Thr-13 hCT), and in the C-terminal region (phospho-Thr-21 hCT) of native hCT were phosphorylated and their fibrillation evaluated.

Phosphorylation at Thr13 in the central region of hCT and located just before the fibrillation-prone D₁₅FNKF₁₉ sequence (15,17,20) resulted in complete inhibition of fibrillation, as indicated by the absence of ThioT and turbidity signals (Figs. 6 and S7). Pulsed HDX-MS showed no significant change in deuterium exposure between 0 and 1440 min and a single deuterated mass envelope at 1440 min (Fig. S9), indicating that phospho-Thr-13 hCT remained stable in monomeric form for 24 h under fibrillating conditions. Previous studies have shown that favorable intermolecular electrostatic interactions between the charged side chains of Asp15 (-1) and Lys18 (+1) residues, together with π - π stacking interactions of Phe16 and Phe19, cause association of hCT in the nucleation step and play an important role in forming antiparallel β -sheet fibrils at neutral pH (15,17,18). Phosphorylation at Thr13 may interfere with these interactions. Interestingly, the same study found that under acidic conditions (pH 3.3), the positively charged side chains of Lys18 (+1) and His20 (+1), located close to the central β -strand structure and facing the same side, prevented monomers from associating with the β -sheet and delayed fibril maturation (18). Here, repulsive intermolecular electrostatic interactions mediated through the negatively charged side chains of phospho-Thr13 and Asp15, located close to the fibrillation-prone central region, may destabilize the π - π stacking interactions to inhibit fibrillation at neutral pH. Strong electrostatic repulsion between negatively charged insulin molecules has previously been shown to disrupt the hydrogen-bonded cross- β networks resulting in dissociation of mature insulin fibrils that were incubated in buffered alkaline solutions (57). Previous studies in our lab have demonstrated that phosphorylation inhibits fibrillation and improves the solubility and stability of glucagon, a fibrillation-prone peptide hormone used to treat hypoglycemia (58). On injection, the phosphate moiety is expected to be cleaved by abundant phosphatases in vivo, regenerating native glucagon (58). Reversible peptide modifications such as phosphorylation can serve as a tool in the rational design of fibrillation-resistant therapeutic peptides such as hCT, and the results presented here demonstrate that phospho-Thr-13 hCT is a promising candidate for future development.

The ThioT and turbidity signals for phospho-Ser-5 hCT were \sim 10-fold weaker than for native hCT (Fig. 6), suggesting the formation of oligomeric intermediates and/or protofibrils, which are known to interact more weakly with ThioT than mature fibrils (54). On visual inspection, phospho-Ser-5 hCT showed thin translucent deposits at the bottom of the microtiter plate, whereas hCT showed solid dense deposits. The weaker ThioT and turbidity intensities, along with the appearance of these deposits, suggest that phosphorylation of Ser5 in the N-terminal loop interferes with fibrillation but does not prevent it (Fig. 6; Table S1). This result further supports the idea that the N-terminal residues are involved in the early nucleation and growth of hCT fibrils (Fig. 3).

Phosphorylation at Thr21 introduces negative charge in the C-terminal region of hCT, just after the fibrillation-prone D₁₅FNKF₁₉ sequence. The ThioT fluorescence results for phospho-Thr-21 hCT showed a greater lag time and an incomplete growth phase relative to hCT (Fig. 6; Table S1), suggesting that phosphorylation of Thr21 delays fibril formation and growth but again does not prevent it entirely. Although phosphorylation at Thr13 and Thr21 introduced negative charge on either side of the fibrillation-prone Renawala et al.

central D₁₅FNKF₁₉ sequence, inhibition of fibrillation was achieved for phospho-Thr-13 hCT, whereas fibrillation was only delayed for phospho-Thr-21 hCT. These results support the idea that the site of phosphorylation is important for inhibiting peptide fibrillation. As shown here, HDX-MS with proteolytic digestion can be used to identify the regions responsible for interactions during the early stages of fibril formation, providing key structural details that can inform the selection of phosphorylation sites.

Disulfide bonds are thought to reduce conformational dynamics and restrict backbone flexibility in fibrillating peptides, influencing the aggregation of their highly aggregation-prone sequence stretches (29,34,35). The Cys1-Cys7 disulfide bond in native hCT constrains the N-terminus into a loop (15). Reducing the disulfide bond relaxes this constraint and allows greater conformational flexibility at the N-terminus. The fibrillation kinetics of native and rhCT, as monitored by ThioT fluorescence and turbidity measurements, showed sigmoidal behavior, with lag, growth, and equilibrium phases characteristic of nucleation-dependent fibrillation (Fig. 1; (51)). Such behavior has been reported previously for native hCT at neutral pH (59). The fibrillation of hCT has been described by a two-step autocatalytic reaction mechanism (14,19,60). The first step is homogeneous nucleation involving self-association of monomers to form oligomeric intermediates or prefibrillar aggregates during the lag phase. The second step is heterogeneous fibrillation involving the association of nuclei and monomers, leading to the elongation of fibrils during the growth phase. The reduction of the Cys1-Cys7 disulfide bond resulted in faster fibrillation of rhCT compared with hCT, with a shorter, almost nonexistent, lag phase followed by rapid fibril growth (Fig. 1). The lag times for rhCT fibrillation measured by ThioT fluorescence and turbidity were $\sim 5 \times$ and $\sim 8 \times$ shorter, respectively, than for hCT fibrillation (Table 1). These results suggest that the reduction of the disulfide bond in native hCT accelerates the formation of nuclei during the lag phase. Cleaving the disulfide bond in therapeutic peptides such as somatostatin, amylin, and insulin has been reported to accelerate fibrillation by increasing the conformational flexibility of the aggregating monomers (32– 36,61). Contrary to the reduced aggregation observed for phospho-Ser-5 hCT, which is also modified in the N-terminal region, rhCT showed a greater tendency to fibrillate. Unlike phosphorylation, which modified the Ser5 residue to introduce charge, reduction of the disulfide bond changed the secondary structure without changing the amino acid sequence.

HDX-MS at the intact level can distinguish the different conformations of monomers, oligomers, and protofibrillar intermediates by their different protection patterns (46). Monomeric species are highly solvent exposed and typically show maximal deuterium incorporation, whereas protein-protein interactions in oligomeric intermediates or mature fibrils provide greater protection from exchange (46). For fibrillating rhCT, HDX-MS results at the intact level showed three distinct populations, whereas only two populations

were detected for hCT (Figs. 2 A and 4 A). This suggests that during fibrillation, rhCT may form intermediates that are structurally different from those formed during fibrillation of hCT and thus that fibrillation of rhCT and hCT proceed by different mechanisms and not merely at different rates. Alternatively, the difference may be attributable to the formation of transient intermediates during rhCT fibrillation that escape detection during hCT fibrillation. Oligomeric intermediates with various secondary structures, including random coil, α -helix, and β -turn, have been reported for calcitonin fibrillation, which highlights the interconverting and heterogeneous nature of early aggregates (59,62–64). The relative populations of different precursor states have been correlated with different morphologies of mature fibrils in vitro (65). Different secondary structures in fibrils of native and disulfide-reduced forms of insulin and somatostatin have been observed using CD spectroscopy and Fourier-transform infrared (FTIR) spectroscopy (34,66). Here, CD spectra showed reduction in random coil intensity during fibrillation consistent with a loss in soluble monomer fraction but did not show structured intermediates or differences in the secondary structures of prefibrillar or fibrillar states of hCT and rhCT (Fig. S1). However, HDX-MS showed differences in the various aggregated assemblies during hCT and rhCT fibrillation based on their different exchange patterns (Figs. 2 and 4).

Proteolytic digestion followed by HDX-MS can be used to identify the regions involved in the early stages of fibrillation (43,46). Numerous studies have implicated the central sequence D₁₅FNKF₁₉ as a key mediator of calcitonin fibrillation. D₁₅FNKF₁₉ is thought to form the core of hCT fibrils, with the side chain phenyl rings of Phe16 and Phe19 involved in stabilizing π - π stacking interactions that provide favorable energetic contributions that help drive fibril self-assembly (14,15,17,20). The central fragment 12-19 in hCT and rhCT, which includes the fibrillation-prone D₁₅FNKF₁₉ sequence, showed an early decrease in deuterium incorporation and greater protection from exchange in the mature fibrils (Figs. 3 A, 5 A, S4, and S6), indicating that this region is involved in the early stages of fibrillation and is incorporated in the core of mature fibrils in both peptides. For rhCT, the central fragment 9–15, which lies just before the amyloidogenic sequence D₁₅FNKF₁₉, showed deuterium uptake kinetics similar to fragment 12–19, suggesting that the 9–15 fragment also participates in the early stages of rhCT fibrillation and may also be amyloidogenic (Figs. 5 A and S6).

The role of the disulfide-bridged N-terminal residues in the fibrillation of native hCT is not well understood. The N-terminal hCT sequence, T₆CMLGT₁₁, has been predicted to be aggregation prone, and its alanine analog (T₆AMLGT₁₁) forms amyloid fibrils at pH 5.5, though the relevance of this fragment to the fibrillation of native hCT (1–32) remains to be determined (67). The HDX-MS results presented here showed early changes in deuterium exposure and a significant decrease in deuteration at 1440 min for hCT fragments 1–8

and 1–11, indicating that the N-terminal residues do play a role in the early nucleation and growth events of hCT fibrillation (Figs. 3 A and S4). Reduction of the disulfide bond produced subtle differences in the fibrillation behaviors of hCT and rhCT at their N-terminal and central regions. For rhCT, the central region (9-19) showed a rapid decrease in deuterium uptake relative to the N-terminus (1–8) during the early stages of fibrillation (0–120 min) (Fig. 5 A), whereas both regions showed similar decreases in deuterium uptake during hCT fibrillation (Fig. 3 A). Interestingly, the N-terminal and central fragments of both hCT and rhCT showed similar overall decreases in deuterium incorporation at 1440 min, with near-complete shifts in their deuterated mass envelopes toward a fully protected population (Figs. S4 and S6). These results suggest that although the N-terminal and central regions of hCT and rhCT differ in their involvement in the early nucleation and growth phases, they are incorporated in the mature fibrils to the same extent in the two peptides.

The lower deuterium uptake at the intact level for rhCT (18%) compared with hCT (28%) at 1440 min suggests that a greater portion of the rhCT sequence is incorporated in the mature fibrils (Figs. 2 A and 4 A). Deuterium uptake results for the C-terminal fragments 20-32 and 26-32 of hCT and rhCT show that there is greater involvement of C-terminal residues in mature fibrils of rhCT as compared with hCT (Figs. 3 A and 5 A). Deuterium uptake for C-terminal fragments 20-32 and 26-32 of rhCT decreased from 62 to 34% and 59 to 36% (Fig. S6), respectively, from 0 to 1440 min, whereas the corresponding hCT fragments did not show a significant decrease during this period (Fig. S4). The deuterated mass envelopes of these rhCT fragments were bimodal (Fig. S6), whereas the corresponding hCT fragments showed minor peak broadening and a limited decrease in deuterium incorporation (Fig. S4). These results suggest that the destabilizing effects of disulfide bond reduction at the N-terminus propagate toward the Cterminus, resulting in greater involvement of C-terminal residues in mature fibrils of rhCT.

CONCLUSIONS

Pulsed HDX-MS, far-UV CD spectroscopy, ThioT fluorescence, and turbidity measurements were used to study the effects of structural modifications on the fibrillation of hCT. Pulsed HDX-MS with proteolytic digestion showed that the N-terminal (1–11) and central (12–19) regions of native hCT are involved in the early stages of hCT fibrillation, whereas the C-terminus (20-32) showed limited participation in mature fibrils. This information was used to develop three phCT analogs that showed modified fibrillation behavior. Phosphorylation at Thr13 resulted in complete inhibition of fibrillation. Phosphorylation at Ser5 interfered with fibrillation and formed translucent oligomeric deposits with weak ThioT fluorescence signal, whereas phosphorylation at Thr21 delayed fibril formation and growth but again did not prevent fibrillation. Reduction of the Cys1-Cys7 disulfide bond affected early nucleation events involving the N-terminal and central regions, resulting in faster fibrillation relative to native hCT. The destabilizing effects of disulfide bond reduction at the N-terminus propagate toward the C-terminus, and the C-terminal residues of rhCT show greater involvement in mature fibrils than comparable residues of native hCT. Together, these findings demonstrate that small changes in the native structure of hCT have a profound effect on its fibrillation behavior and that an understanding of these effects can be exploited to produce fibrillation-resistant analogs.

SUPPORTING MATERIAL

Supporting Material can be found online at https://doi.org/10.1016/j.bpj. 2020.11.009.

AUTHOR CONTRIBUTIONS

H.K.R. performed the studies and analyzed the HDX-MS and kinetic data. K.B.C. performed and analyzed the data for the CD spectroscopy studies. H.K.R. drafted the manuscript, and all authors commented and contributed to the revisions. E.M.T. supervised the project, designed the studies and analyzed the data in collaboration with H.K.R. and K.B.C., and oversaw the data analysis and manuscript preparation.

ACKNOWLEDGMENTS

The authors acknowledge Drs. Suzanne M. D'Addio and Katelyn J. Smith for helpful discussions on therapeutic peptide fibrillation.

This research was supported in part by National Institutes of Health (NIH) grant R01 GM085293 (Principal Investigator: E.M.T.) and by the Trask Trust Fund, Purdue University, West Lafayette, IN (Principal Investigator: E.M.T.).

REFERENCES

- 1. Felsenfeld, A. J., and B. S. Levine. 2015. Calcitonin, the forgotten hormone: does it deserve to be forgotten? Clin. Kidney J. 8:180–187.
- 2. Kamgar-Parsi, K., J. Tolchard, ..., A. Ramamoorthy. 2017. Structural biology of calcitonin: from aqueous therapeutic properties to amyloid aggregation. Isr. J. Chem. 57:634-650.
- 3. Chesnut, C. H., III, M. Azria, ..., L. Mindeholm. 2008. Salmon calcitonin: a review of current and future therapeutic indications. Osteoporos. Int. 19:479-491.
- 4. Zaidi, M., A. M. Inzerillo, ..., P. Burckhardt. 2002. Molecular and clinical pharmacology of calcitonin. In Principles of Bone Biology. J. P. Bilezikian, L. G. Raisz, and G. A. Rodan, eds. Elsevier, pp. 1423-1440.
- 5. Manicourt, D. H., J. P. Devogelaer, ..., S. Silverman. 2005. Rationale for the potential use of calcitonin in osteoarthritis. J. Musculoskelet. Neuronal Interact. 5:285-293.
- 6. Lyles, K. W., E. S. Siris, ..., P. J. Meunier. 2001. A clinical approach to diagnosis and management of Paget's disease of bone. J. Bone Miner. Res. 16:1379-1387.
- 7. Moussa, E. M., J. P. Panchal, ..., E. M. Topp. 2016. Immunogenicity of therapeutic protein aggregates. J. Pharm. Sci. 105:417-430.
- 8. Grauer, A., H. H. Reinel, ..., F. Raue. 1993. Neutralizing antibodies against calcitonin. Horm. Metab. Res. 25:486-488.

Please cite this article in press as: Renawala et al., Fibrillation of Human Calcitonin and Its Analogs: Effects of Phosphorylation and Disulfide Reduction, Biophysical Journal (2021), https://doi.org/10.1016/j.bpj.2020.11.009

Renawala et al.

- Shimizu, N., and Y. Oomura. 1986. Calcitonin-induced anorexia in rats: evidence for its inhibitory action on lateral hypothalamic chemosensitive neurons. *Brain Res.* 367:128–140.
- Singer, F. R., R. S. Fredericks, and C. Minkin. 1980. Salmon calcitonin therapy for Paget's disease of bone. The problem of acquired clinical resistance. *Arthritis Rheum*. 23:1148–1154.
- Singer, F. R., J. P. Aldred, ..., K. J. Bloch. 1972. An evaluation of antibodies and clinical resistance to salmon calcitonin. *J. Clin. Invest.* 51:2331–2338.
- Cudd, A., T. Arvinte, ..., I. MacIntyre. 1995. Enhanced potency of human calcitonin when fibrillation is avoided. J. Pharm. Sci. 84:717–719.
- Fowler, S. B., S. Poon, ..., J. Zurdo. 2005. Rational design of aggregation-resistant bioactive peptides: reengineering human calcitonin. *Proc. Natl. Acad. Sci. USA*. 102:10105–10110.
- Kamihira, M., A. Naito, ..., H. Saitô. 2000. Conformational transitions and fibrillation mechanism of human calcitonin as studied by high-resolution solid-state 13C NMR. *Protein Sci.* 9:867–877.
- Naito, A., M. Kamihira, ..., H. Saitô. 2004. Structural diversity of amyloid fibril formed in human calcitonin as revealed by site-directed 13C solid-state NMR spectroscopy. *Magn. Reson. Chem.* 42:247–257.
- Itoh-Watanabe, H., M. Kamihira-Ishijima, ..., A. Naito. 2013. Characterization of the spherical intermediates and fibril formation of hCT in HEPES solution using solid-state 13C-NMR and transmission electron microscopy. *Phys. Chem. Chem. Phys.* 15:16956–16964.
- Itoh-Watanabe, H., M. Kamihira-Ishijima, ..., A. Naito. 2013. Role of aromatic residues in amyloid fibril formation of human calcitonin by solid-state 13C NMR and molecular dynamics simulation. *Phys. Chem. Chem. Phys.* 15:8890–8901.
- Kamihira, M., Y. Oshiro, ..., A. Naito. 2003. Effect of electrostatic interaction on fibril formation of human calcitonin as studied by high resolution solid state 13C NMR. J. Biol. Chem. 278:2859–2865.
- Kanaori, K., and A. Y. Nosaka. 1995. Study of human calcitonin fibrillation by proton nuclear magnetic resonance spectroscopy. *Biochemistry*. 34:12138–12143.
- Reches, M., Y. Porat, and E. Gazit. 2002. Amyloid fibril formation by pentapeptide and tetrapeptide fragments of human calcitonin. *J. Biol. Chem.* 277:35475–35480.
- Lakshmanan, A., D. W. Cheong, ..., C. A. Hauser. 2013. Aliphatic peptides show similar self-assembly to amyloid core sequences, challenging the importance of aromatic interactions in amyloidosis. *Proc. Natl. Acad. Sci. USA*. 110:519–524.
- Bertolani, A., A. Pizzi, ..., P. Metrangolo. 2017. Crystal structure of the DFNKF segment of human calcitonin unveils aromatic interactions between phenylalanines. *Chemistry*. 23:2051–2058.
- 23. Gazit, E. 2002. A possible role for π -stacking in the self-assembly of amyloid fibrils. *FASEB J.* 16:77–83.
- 24. Epand, R. M., R. F. Epand, ..., G. L. Stahl. 1985. A comparison of the interaction of glucagon, human parathyroid hormone-(1-34)-peptide and calcitonin with dimyristoylphosphatidylglycerol and with dimyristoylphosphatidylcholine. *Biophys. Chem.* 23:39–48.
- Stroop, S. D., H. Nakamuta, ..., R. M. Epand. 1996. Determinants for calcitonin analog interaction with the calcitonin receptor N-terminus and transmembrane-loop regions. *Endocrinology*. 137:4752–4756.
- Rawat, A., and D. Kumar. 2013. NMR investigations of structural and dynamics features of natively unstructured drug peptide - salmon calcitonin: implication to rational design of potent sCT analogs. *J. Pept. Sci.* 19:33–45.
- Orlowski, R. C., R. M. Epand, and A. R. Stafford. 1987. Biologically potent analogues of salmon calcitonin which do not contain an N-terminal disulfide-bridged ring structure. Eur. J. Biochem. 162:399–402.
- Goltzman, D. 1980. Examination of interspecies differences in renal and skeletal receptor binding and adenylate cyclase stimulation with human calcitonin. *Endocrinology*. 106:510–518.
- Fass, D. 2012. Disulfide bonding in protein biophysics. *Annu. Rev. Bio-phys.* 41:63–79.

- **30.** Vaz, D. C., J. R. Rodrigues, ..., R. M. Brito. 2006. Enthalpic and entropic contributions mediate the role of disulfide bonds on the conformational stability of interleukin-4. *Protein Sci.* 15:33–44.
- 31. Betz, S. F. 1993. Disulfide bonds and the stability of globular proteins. *Protein Sci.* 2:1551–1558.
- 32. Ridgway, Z., X. Zhang, ..., D. P. Raleigh. 2018. Analysis of the role of the conserved disulfide in amyloid formation by human islet amyloid polypeptide in homogeneous and heterogeneous environments. *Biochemistry*. 57:3065–3074.
- Ilitchev, A. I., M. J. Giammona, ..., M. T. Bowers. 2016. Human islet amyloid polypeptide N-terminus fragment self-assembly: effect of conserved disulfide bond on aggregation propensity. J. Am. Soc. Mass Spectrom. 27:1010–1018.
- Anoop, A., S. Ranganathan, ..., S. K. Maji. 2014. Elucidating the role
 of disulfide bond on amyloid formation and fibril reversibility of somatostatin-14: relevance to its storage and secretion. *J. Biol. Chem.*289:16884–16903.
- Li, Y., H. Gong, ..., K. Huang. 2012. Dissecting the role of disulfide bonds on the amyloid formation of insulin. *Biochem. Biophys. Res.* Commun. 423:373–378.
- Maeda, R., K. Ado, ..., Y. Taniguchi. 2007. Promotion of insulin aggregation by protein disulfide isomerase. *Biochim. Biophys. Acta*. 1774:1619–1627.
- Maier, R., B. Kamber, ..., W. Rittel. 1976. Analogues of human calcitonin: IV. Influence of leucine substitutios in positions 12, 16 and 19 on hypocalcaemic activity in the rat. Clin. Endocrinol. 5:s327–s332.
- Andreotti, G., R. M. Vitale, ..., A. Motta. 2011. Converting the highly amyloidogenic human calcitonin into a powerful fibril inhibitor by three-dimensional structure homology with a non-amyloidogenic analogue. *J. Biol. Chem.* 286:2707–2718.
- 39. Chen, Y.-T., K.-W. Hu, ..., L.-H. Tu. 2019. Inhibiting human calcitonin fibril formation with its most relevant aggregation-resistant analog. *J. Phys. Chem. B.* 123:10171–10180.
- Kapurniotu, A., R. Kayed, ..., W. Voelter. 1999. Rational design, conformational studies and bioactivity of highly potent conformationally constrained calcitonin analogues. Eur. J. Biochem. 265:606–618.
- Illes-Toth, E., D. L. Rempel, and M. L. Gross. 2018. Pulsed hydrogendeuterium exchange illuminates the aggregation kinetics of α-synuclein, the causative agent for parkinson's disease. ACS Chem. Neurosci. 9:1469–1476.
- Zhang, Y., D. L. Rempel, ..., M. L. Gross. 2013. Pulsed hydrogendeuterium exchange mass spectrometry probes conformational changes in amyloid beta (Aβ) peptide aggregation. *Proc. Natl. Acad. Sci. USA*. 110:14604–14609.
- Moorthy, B. S., H. T. Ghomi, ..., E. M. Topp. 2015. Structural transitions and interactions in the early stages of human glucagon amyloid fibrillation. *Biophys. J.* 108:937–948.
- 44. Kheterpal, I., M. Chen, ..., R. Wetzel. 2006. Structural differences in Abeta amyloid protofibrils and fibrils mapped by hydrogen exchange-mass spectrometry with on-line proteolytic fragmentation. *J. Mol. Biol.* 361:785–795.
- 45. Nakazawa, S., N. Hashii, ..., N. Kawasaki. 2013. Analysis of the local dynamics of human insulin and a rapid-acting insulin analog by hydrogen/deuterium exchange mass spectrometry. *Biochim. Biophys.* Acta. 1834:1210–1214.
- Kheterpal, I., and R. Wetzel. 2006. Hydrogen/deuterium exchange mass spectrometry–a window into amyloid structure. Acc. Chem. Res. 39:584–593.
- Brown, K. A., and D. J. Wilson. 2017. Bottom-up hydrogen deuterium exchange mass spectrometry: data analysis and interpretation. *Analyst* (*Lond.*). 142:2874–2886.
- 48. Kostyukevich, Y., T. Acter, ..., E. Nikolaev. 2018. Hydrogen/deuterium exchange in mass spectrometry. *Mass Spectrom. Rev.* 37:811–853.
- **49.** Biancalana, M., K. Makabe, ..., S. Koide. 2009. Molecular mechanism of thioflavin-T binding to the surface of beta-rich peptide self-assemblies. *J. Mol. Biol.* 385:1052–1063.

- 50. Khurana, R., C. Coleman, ..., S. Singh. 2005. Mechanism of thioflavin T binding to amyloid fibrils. J. Struct. Biol. 151:229-238.
- 51. Zhang, J., X. Mao, and W. Xu. 2018. Fibril nucleation kinetics of a pharmaceutical peptide: the role of conformation stability, formulation factors, and temperature effect. Mol. Pharm. 15:5591-5601.
- 52. Masson, G. R., J. E. Burke, ..., K. D. Rand. 2019. Recommendations for performing, interpreting and reporting hydrogen deuterium exchange mass spectrometry (HDX-MS) experiments. Nat. Methods. 16:595-602.
- 53. Kammari, R., and E. M. Topp. 2019. Solid-state hydrogen-deuterium exchange mass spectrometry (sshdx-ms) of lyophilized poly-d,lalanine. Mol. Pharm. 16:2935-2946.
- 54. Gade Malmos, K., L. M. Blancas-Mejia, ..., D. Otzen. 2017. ThT 101: a primer on the use of thioflavin T to investigate amyloid formation. Amyloid, 24:1–16.
- 55. Sawaya, M. R., S. Sambashivan, ..., D. Eisenberg. 2007. Atomic structures of amyloid cross- β spines reveal varied steric zippers. *Nature*. 447:453-457.
- 56. D'Addio, S. M., J. R. Bothe, ..., A. C. Templeton. 2016. New and evolving techniques for the characterization of peptide therapeutics. J. Pharm. Sci. 105:2989-3006.
- 57. Shammas, S. L., T. P. Knowles, ..., G. L. Devlin. 2011. Perturbation of the stability of amyloid fibrils through alteration of electrostatic interactions. Biophys. J. 100:2783-2791.
- 58. Topp, E. M. M., H. T. Ghomi, ..., S. M. Balakrishnan. 2019. Modified glucagon molecules. US patent US10308701B2, filed July 22, 2016, and published January 26, 2017.
- 59. Kamgar-Parsi, K., L. Hong, ..., A. Ramamoorthy. 2017. Growthincompetent monomers of human calcitonin lead to a noncanonical

- direct relationship between peptide concentration and aggregation lag time. J. Biol. Chem. 292:14963-14976.
- 60. Arvinte, T., A. Cudd, and A. F. Drake. 1993. The structure and mechanism of formation of human calcitonin fibrils. J. Biol. Chem. 268:6415-6422.
- 61. Huang, K., N. C. Maiti, ..., M. A. Weiss. 2006. Structure-specific effects of protein topology on cross-β assembly: studies of insulin fibrillation. Biochemistry. 45:10278-10293.
- Avidan-Shpalter, C., and E. Gazit. 2006. The early stages of amyloid formation: biophysical and structural characterization of human calcitonin pre-fibrillar assemblies. Amyloid. 13:216-225.
- 63. Diociaiuti, M., G. Macchia, ..., F. Malchiodi-Albedi. 2014. Native metastable prefibrillar oligomers are the most neurotoxic species among amyloid aggregates. Biochim. Biophys. Acta. 1842:1622-1629.
- 64. Huang, R., S. Vivekanandan, ..., A. Ramamoorthy. 2012. NMR characterization of monomeric and oligomeric conformations of human calcitonin and its interaction with EGCG. J. Mol. Biol. 416:108-120.
- 65. Smith, D. P., S. Jones, ..., S. E. Radford. 2003. A systematic investigation into the effect of protein destabilisation on beta 2-microglobulin amyloid formation. J. Mol. Biol. 330:943-954.
- 66. Zako, T., M. Sakono, ..., M. Maeda. 2009. Bovine insulin filaments induced by reducing disulfide bonds show a different morphology, secondary structure, and cell toxicity from intact insulin amyloid fibrils. Biophys. J. 96:3331-3340.
- 67. Iconomidou, V. A., A. Leontis, ..., S. J. Hamodrakas. 2013. Identification of a novel 'aggregation-prone'/'amyloidogenic determinant' peptide in the sequence of the highly amyloidogenic human calcitonin. FEBS Lett. 587:569-574.